Journal of Solid State Chemistry 182 (2009) 896–904

Contents lists available at ScienceDirect

Journal of Solid State Chemistry

journal homepage: www.elsevier.com/locate/jssc

The crystal structure of $Hf_{1.5+\delta}Nb_{1.5-\delta}As$ and structure–composition relations in the section Hf_3As–Nb_3As

Piotr Warczok, Igor Chumak [1], Klaus W. Richter *

Department of Inorganic Chemistry/Materials Chemistry, University of Vienna, Waehringerstr. 42, A-1090 Wien, Austria

ARTICLE INFO

Article history:
Received 21 November 2008
Received in revised form
14 January 2009
Accepted 18 January 2009
Available online 24 February 2009

Keywords:
As–Hf–Nb system
Transition metal arsenides
Crystal structure
Partial ordering
First principles
Thermodynamic model

ABSTRACT

The title compound $Hf_{1.5+\delta}Nb_{1.5-\delta}As$ was characterized by means of single crystal X-ray diffraction. It represents a new structure type of intermetallic compounds (space group *Pnma*; lattice parameters $a = 7.142(2)$ Å, $b = 3.583(2)$ Å, $c = 11.640(2)$ Å) and shows a small homogeneity range corresponding to $(0.1 < \delta < 0.25)$ at 1400 °C. The crystal structure may be visualized by a combination of As-centred trigonal prisms of the metal atoms and bcc-like fragments formed by metal atoms. Structural relations with various binary arsenides are discussed. The structure of $Hf_{1.5+\delta}Nb_{1.5-\delta}As$ shows significant preferred site occupation of Hf and Nb at the three independent metal positions (differential fractional site occupancy). Structure–composition relations in the section Hf_3As–Nb_3As which also contains the new phase $Hf_{2+\delta}Nb_{1-\delta}As$ with Ti_3P-type structure (space group $P4_2/n$) are discussed. Ground state energies of various ordered compounds with $Hf_{1.5+\delta}Nb_{1.5-\delta}As$-, Ti_3P- and Ta_3As-type structures were calculated from ab initio density functional theory. These energies were used for thermodynamic calculations employing the compound energy formalism (CEF) with the aim to model the experimentally observed site fraction data for both ternary compounds as well as Gibbs energies at the temperature of equilibration (1400 °C).

1. Introduction

The arsenides of Hf and Nb have been structurally characterized beginning in the year 1962. While the arsenic-rich compounds with MAs and MAs_2 stoichiometry can be synthesized by direct reaction of the pure metal powders with As-vapour at moderate temperatures around 1000 °C [1,2], the metal-rich arsenides are only accessible via high temperature routes, like the arc melting of powder mixtures containing the pre-reacted mono- and diarsenides. Five metal-rich compounds were reported to exist in the Hf–As system [3,4]: Hf_3As_2 (S_3Sb_2-type, *Pnma*), Hf_5As_3 (Nb_5As_3-type, *Pnma*), Hf_7As_4 (Nb_7P_4-type, *C*2/*m*), Hf_2As (Ta_2P-type, *Pnnm*) and Hf_3As (Ta_3As-type, *C*2/*c*). In the Nb–As system, four metal-rich compounds were found: Nb_4As_3 (Nb_4As_3-type, *Cmcm*) [5], Nb_5As_3 (Nb_5As_3-type, *Pnma*) [6], Nb_7As_4 (Nb_7P_4-type, *C*2/*m*) [7] and Nb_3As (Ti_3P-type, $P4_2/n$) [8]. Crystal structure information for the two phases Hf_3As and Nb_3As which are relevant for the current study is given in Tables 1 and 2.

The ternary system Hf–Nb–As has not been investigated up to now, but given the similar chemical properties of Hf and Nb, considerable substitution in the binary structures is to be expected. On the other hand, partial ordering of different but similar transition metals often leads to the formation of new ternary compounds according to the *differential fractional site occupancy* (DFSO) *concept*, which was originally formulated for mixed Nb/Ta sulfides [9]. The application of this concept led to the discovery of many new ternary pnictides and chalcogenides of the early transition metals in recent years [10], including some new ternary arsenides like $(Ti,Mo)_5As_3$ with Yb_5Bi_3-type structure (*Pnma*) [11], Ti_2MoAs_2 (V_3As_2-type, $P4/m$) and Ti_3MoAs_3 (Cr_4As_3-type, *C*2/*m*) [12].

Different approaches that have been used to rationalize the site preferences in DFSO stabilized compounds and partially ordered solid solutions are discussed in Ref. [13]. This includes basic site volume considerations, site potential analysis based on atomic orbital populations (AOPs) and the analysis of the bonding situation employing electronic structure calculations or the application of Pauling bond orders (PBOs). Usually a combination of different driving forces is needed to rationalize the experimentally observed site preferences in DFSO stabilized compounds, which is also reflected in our own previous studies of various DFSO stabilized germanides found in the system Ta–Zr–Ge [14,15]. Recently we successfully used a different approach to predict the preferred site occupation for solid solutions in the Hf–Nb–Ge [16,17] and Hf–Zr–Ge [18] systems. This was done by using ground state energies of hypothetical ordered compounds (obtained from

* Corresponding author. Fax: +431 4277 9529.
E-mail address: klaus.richter@univie.ac.at (K.W. Richter).
[1] Present address: IWF Dresden, Institut für Komplexe Materialien, Helmholtzstr. 20, 01069 Dresden, Germany.

0022-4596/$ - see front matter © 2009 Elsevier Inc. All rights reserved.
doi:10.1016/j.jssc.2009.01.020

Table 1
Crystal structure data for Hf_3As according to Ref. [4].

Structure type		Ta_3As		
Space group		*C*2/*c*		
Cell parameters (Å)				
a		15.3898(14)		
b		5.3795(5)		
c		15.3330(14)		
β (°)		90.291(6)		
Atomic position	Wyckoff number	Coordinates		
		x	*y*	*z*
Hf1	8*f*	0.7367(5)	0.7895(12)	0.4026(6)
Hf2	8*f*	0.1570(5)	0.7231(15)	0.5100(5)
Hf3	8*f*	0.9415(5)	0.4802(15)	0.1669(5)
Hf4	8*f*	0.0808(5)	0.9664(14)	0.6899(5)
Hf5	8*f*	0.7362(5)	0.2672(13)	0.3021(5)
Hf6	8*f*	0.9487(5)	0.7556(14)	0.4835(5)
As1	8*f*	0.9161(9)	0.9916(35)	0.1317(10)
As2	8*f*	0.1214(9)	0.4602(31)	0.6627(12)

Table 2
Crystal structure data for Nb_3As according to Ref. [8].

Structure type		Ti_3P		
Space group		$P4_2/n$		
Lattice parameters (Å)				
a		10.294(4)		
c		5.199(2)		
Atomic position	Wyckoff number	Coordinates		
		x	*y*	*z*
Nb1	8*f*	0.4152(1)	0.9054(1)	0.9772(2)
Nb2	8*f*	0.3521(1)	0.5117(1)	0.7681(2)
Nb3	8*f*	0.3062(1)	0.7864(1)	0.4911(1)
As1	8*f*	0.2930(1)	0.5214(1)	0.2703(3)

DFT calculations) for thermodynamic modelling in the framework of the compound energy formalism (CEF). It was shown that this type of modelling can be used to describe the experimentally observed site occupations in these solid solutions with high accuracy.

The current work is part of a larger project with the aim to study the effects of partial ordering in metal-rich gallides, germanides and arsenides on a broad experimental basis. We report on the synthesis and structural characterization of the new ternary compound $Hf_{1.5+\delta}Nb_{1.5-\delta}As$ (own structure type, *Pnma*) stabilized by DFSO. A theoretical study of site occupations and total energies within the section Hf_3As–Nb_3As based on first principle calculations and the thermodynamic modelling was performed, and the calculations are discussed in the light of experimental results.

2. Methods

2.1. Synthesis and analyses

The samples were prepared from Hf powder (Alfa Aesar, containing 2–3.5% Zr, content of Hf+Zr metal basis 99.6%), Nb powder (Alfa Aesar with a content of Ta < 500 ppm, content of Nb+Ta metal basis 99.99%) and As polycrystalline lumps (Johnson Matthey, 99.9999%). The materials were stored and handled in the glove-box in order to avoid a longer exposition to air. Before use, the arsenic lumps were heated in a silica tube under dynamic vacuum, in order to remove any arsenic oxides from the surface.

In a first step, the monoarsenides HfAs and NbAs were prepared from stoichiometric amounts of the metal powders and arsenic lumps. The elements were sealed into an evacuated silica tube, heating to 900 °C within 2 days, and then annealing at this temperature for 3 days. The obtained powder was re-heated in a dynamic vacuum to decompose remaining diarsenides. The powder X-ray patterns of these products showed some weak diffraction lines of the diarsenides, but no trace of the oxide or silicide phases. Calculated amounts of the prepared monoarsenides and metal powders were weighed to a sample mass of 1000 mg. All mixtures were mixed and pressed to pellets with a diameter of 5 mm which were subsequently melted in the arc-furnace under an argon atmosphere. Due to the high vapour pressure of As and the high melting point of the metal-rich ternary alloys, considerable amounts of As evaporated during arc melting and mass losses in the order of 3–30 mg (depending on the starting composition) were observed.

The arc melted samples were sealed in closed tantalum crucibles under 0.5 bar Ar, annealed at 1400 °C for 3 days and quenched in a water-cooled steel vessel under argon.

Initial sample characterization was performed by X-ray powder diffraction using a Bruker AXS D8 powder diffractometer in Bragg–Brentano reflection setting and Cu*K*α-radiation. Phase identification and pattern refinement was performed with the Topas Software [19] applying the fundamental parameter approach for peak profile modelling.

Pieces of the annealed samples were cut with a diamond saw, embedded in resin, ground and polished for metallographic investigation of the microstructure by optical light microscopy.

The phase compositions were analysed by EPMA on a Cameca SX electron probe 100 using wavelength dispersive spectroscopy (WDS) for quantitative analyses and employing pure hafnium, niobium and GaAs as standard materials. The measurements were carried out at 20 kV and a beam current of 20 nA using the Hf(Mα), Nb(Lα) and As(Lβ) emission lines for intensity measurements. Conventional ZAF matrix correction was used to calculate the final compositions from the measured X-ray intensities.

The single crystals for structure determination were separated from the bulk sample under an optical microscope. Diffraction data were collected on a Bruker SMART CCD diffractometer equipped with a CCD detector and a 300 μm capillary-optics collimator (Mo tube, graphite monochromator). The unit-cell parameters were obtained by least-squares refinements of 2ϑ values. Corrections for Lorentz, polarization and absorption effects were done by application of the multi-scan method [20]. The structure solution by direct methods and subsequent structure refinement was performed using the Shelx97 software package [21]. Selected information on single crystal X-ray data collection and refinements are given in Table 3 and the structural parameters are compiled in Table 4.

2.2. Modelling

A detailed discussion of the applied method of modelling was given in Ref. [17]. For the thermodynamic calculations, the CEF [22] was used. The CEF belongs to the group of sublattice models used for the calculation of phase diagrams (CALPHAD method). The term *sublattice* refers to a set of atoms within the unit cell and usually corresponds to one or several symmetrically independent sites. In the CEF model, the Gibbs energy of a solid solution MX is given by

$$G_{MX} = G^{ref}_{MX} - TS^{id}_{MX} + {}^{E}G_{MX} \quad (1)$$

with G^{ref}_{MX} being the frame of reference for the Gibbs energy, S^{id}_{MX} the ideal entropy of mixing and ${}^{E}G_{MX}$ the excess Gibbs energy

(which was neglected in the current study). The frame of reference for the Gibbs energy G_{MX}^{ref} describes the energies of *end members* (i.e. hypothetical compounds with every sublattice occupied by only one element):

$$G_{MX}^{ref} = \sum_I P_I(Y) G_I \quad (2)$$

where I is defined as an array describing an end member, Y a matrix describing the site fractions of all components on all sublattices, $P_I(Y)$ is the product of site fractions from Y corresponding to the end member described by I and G_I the Gibbs energy of the end member described by I. The ideal entropy of mixing describes the contribution of the random mixing on each sublattice and is given by

$$S_{MX}^{id} = -R \sum_i a^i \sum_j y_j^i \sum_i \ln y_j^i \quad (3)$$

with a^i being the stoichiometric contribution of atoms on the sublattice i ($\Sigma a^i = 1$) and y_j^i being the site fraction of the element j on sublattice i.

Knowing the Gibbs energy of all end members, the equilibrium site fractions y_j^i contributing to the frame of reference as well as to the ideal entropy of mixing can be determined by Gibbs energy minimization for a given temperature. These calculations were performed using the Thermo-Calc software package [23]. The thermodynamic descriptions of the reference state phases (As-grey, Hf-hcp and Nb-bcc) were taken from the SGTE database [24].

The end members were defined according to the crystal structures of the ternary phase $Hf_{1.5+\delta}Nb_{1.5-\delta}As$ and the structures of binary Hf_3As and Nb_3As. The ground state energies (at 0 K) were calculated by DFT calculations using the *Vienna Ab initio Simulation Package* (VASP) ver.4.6 [25,26]. The cell parameters and the atomic coordinates were optimized by a conjugate-gradient algorithm [27] in order to determine the ground state energies. The starting structures (lattice parameters and atomic positions) were taken from the experimental crystal structure data as listed in Tables 1–4. The optimal volume was determined by computing the energy for a series of volumes covering an interval of 0.96–1.03 around the calculated equilibrium volume, and fitting these energies to a polynomial. The potentials for Hf, Nb and As were generated with the projector augmented wave method [28,29]. The generalized gradient approximation PBE [30] with a plane wave cut-off energy of 290 eV was applied throughout this work. The integration of the Brillouin Zone was done with Γ-centred Monkhorst-Pack grids [31] of $[3\times6\times2]$ for $Hf_{1.5+\delta}Nb_{1.5-\delta}As$, $[2\times6\times2]$ for Hf_3As, and $[2\times2\times4]$ for Nb_3As. The k-point convergence was examined for the equilibrium ground state structures with grids of $[6\times12\times4]$, $[4\times12\times4]$, and $[4\times4\times8]$, respectively. The tetrahedron method with Blöchl corrections [32] was used to determine the partial occupancy of each one-electron wave function.

Table 3
Crystal data and structure refinements for $Hf_{1.5+\delta}Nb_{1.5-\delta}As$.

Empirical formula	$Hf_{1.7}Nb_{1.3}As$
Formula weight	498.71
Unit cell dimensions	$a = 7.142(2)$ Å $b = 3.583(2)$ Å $c = 11.640(2)$ Å $V = 297.9(2)$ Å^3
Crystal system, space group	Orthorhombic, *Pnma*
Z	4
Calculated density	11.121 Mg/m^3
Absorption coefficient	74.549 mm^{-1}
Crystal dimensions	$30\times30\times50$ μm
Range of data collection	$6.7<2\vartheta<55.0^\circ$
Number of images / rotation angle per image	519/2°
Scan mode (at distinct ω-angles)	φ-scans
Scan time	100 s/°
Detector-to-sample distance	30 mm
Reflections collected /unique	5066/398
Number of refined parameters	29
GooF $= \{\Sigma[w(F_o^2-F_c^2)^2]/(n-p)\}^{1/2}$	1.278
$R1 = \Sigma(\|\|F_o\|-\|F_c\|\|)/\Sigma F_o$	0.0231
$wR2 = [\Sigma w(F_o^2-F_c^2)^2/\Sigma\|wF_o^4]^{1/2}$	0.0625
Extinction coefficient	0.0031(4)
Final difference Fourier map (e Å^{-3})	2.915 to −1.692 e Å^{-3}

3. Results and discussion

3.1. The crystal structure of $Hf_{1.5+\delta}Nb_{1.5-\delta}As$

The title compound was observed in three different ternary samples investigated during our systematic study of the metal-rich part of the Hf–Nb–As system. Details on the complex ternary phase equilibria observed at 1400 °C will be published separately [33]. The phase compositions (EPMA data) and lattice parameters (powder XRD) of $Hf_{1.5+\delta}Nb_{1.5-\delta}As$ are given in Table 6 together with selected values for other phases present in the section Hf_3As–Nb_3As. EPMA results show that the new phase clearly exhibits M_3As stoichiometry and exists in a relatively small composition range $Hf_{1.5+\delta}Nb_{1.5-\delta}As$ ($0.1<\delta<0.25$). Note that the sample compositions given in Table 6 are the nominal compositions calculated considering also the mass loss observed during arc melting. The samples contained M_3As-phases in equilibrium with other ternary phases and a bcc Nb-based solid solution.

A single crystal suitable for structure determination could be isolated from the sample with the nominal composition 40.2% Hf, 39.9% Nb and 19.9 As (compare Table 6). The structure was solved by direct methods in the space group *Pnma* and subsequent refinements yielded the results compiled in Tables 3–5. Further details of the crystal structure investigation can be obtained from the Fachinformationszentrum Karlsruhe, 76344 Eggenstein-Leopoldshafen, Germany (fax: +49 7247 808 666; e-mail: crysdata@fiz.karlsruhe.de) on quoting the depository number CSD 420062. A projection of the crystal structure of $Hf_{1.5+\delta}Nb_{1.5-\delta}As$ in the direction of the short b-axis is given in Fig. 1.

The structural features of $Hf_{1.5+\delta}Nb_{1.5-\delta}As$ can be well described by a combination of trigonal prisms formed from metal atoms (centred by As) and distorted bcc-like fragments of the metal atoms. All trigonal prisms around As are sharing common edges and are stacked on their basal planes in [0 1 0] direction. The metal atoms on the $M1$ site are situated in the centre of a distorted metal cube with M–M distances in the range of 2.88–3.27 Å,

Table 4
Atomic coordinates and equivalent displacement parameters for $Hf_{1.5+\delta}Nb_{1.5-\delta}As$.

Site	Wyckoff position	x	y	z	U(eq) (Å$^2\times10^4$)	Occupation
$M1$	4c	0.0559(1)	1/4	0.5953(1)	82(3)	0.49(1) Nb+0.51(1) Hf
$M2$	4c	0.1551(1)	1/4	0.0181(1)	67(2)	0.75(1) Nb+0.25(1) Hf
$M3$	4c	0.2692(1)	1/4	0.3042(1)	56(3)	0.07(1) Nb+0.93(1) Hf
As3	4c	0.4363(2)	1/4	0.6785(1)	46(5)	1

Table 5
Anisotropic displacement parameters for $Hf_{1.5+\delta}Nb_{1.5-\delta}As$ [$Å^2 \times 10^3$].

Site	U_{11}	U_{22}	U_{33}	U_{23}	U_{13}	U_{12}
*M*1	6(1)	6(1)	9(1)	0	−3(1)	0
*M*2	5(1)	12(1)	8(1)	0	0(1)	0
*M*3	5(1)	7(1)	5(1)	0	1(1)	0
As3	3(1)	5(1)	5(1)	0	0(1)	0

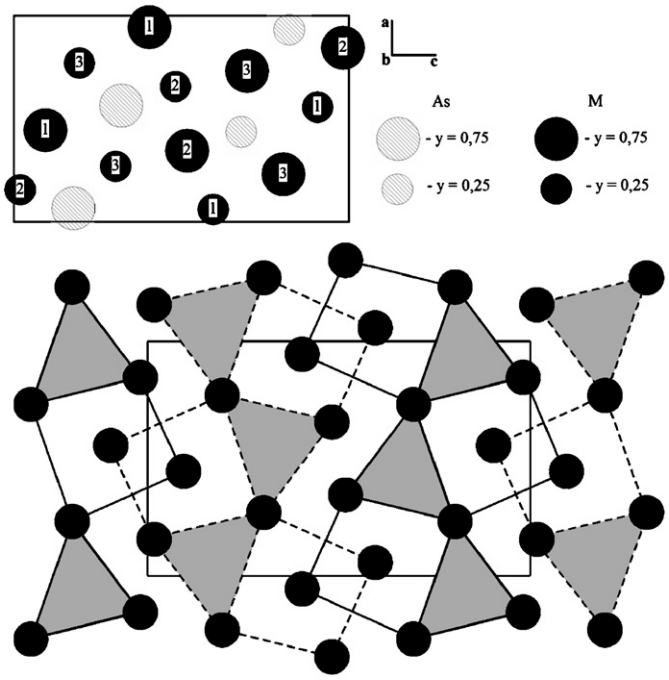

Fig. 1. The crystal structure of $Hf_{1.5+\delta}Nb_{1.5-\delta}As$ (new type, *Pnma*) in [010] direction. Top: Projection of the unit cell with the *M*-sites numbered according to the site designation given in Table 4. Bottom: Arrangement of trigonal prisms in grey and *M*-atoms as black circles. The As-atoms are situated in the centre of the trigonal prisms. The *M*-atoms at $y = 0.25$ are connected with bold lines, at $y = 0.75$—with dashed lines.

which are condensed to columns of two interpenetrating distorted bcc units (Fig. 1, bottom).

A combination of trigonal prisms and bcc fragments is in fact quite common in metal-rich pnictides and such arrangements can be found in the binary compounds Hf_5As_3 and Nb_5As_3 (Nb_5As_3-type, *Pnma*), Hf_7As_4 and Nb_7As_4 (Nb_7P_4-type, *C*2/*m*) and in Hf_2As (Ta_2P-type, *Pnnm*) shown in Fig. 2. In all these structure types, several different As-sites are present, so the arrangement of trigonal prisms and their interconnection is more complicated as for $Hf_{1.5+\delta}Nb_{1.5-\delta}As$. The bcc-fragments are isolated in case of the Nb_5As_3- and Nb_7P_4-type structures, while the more metal-rich Ta_2P-type structure exhibits two condensed bcc-units sharing a common face.

Interestingly, the two binary compounds with M_3As stoichiometry, Hf_3As (Ta_3As-type, *C*2/*c*) and Nb_3As (Ti_3P-type, $P4_2/n$), do not belong to this series of structure types. The two closely related structures have already been discussed by Willerström et al. [4]. The metal atoms around As form distorted square antiprisms sharing a common edge or a common vertex to form a three-dimensional network which do not contain any distorted bcc-fragments (Fig. 3).

On the first sight, the atomic arrangement in $Hf_{1.5+\delta}Nb_{1.5-\delta}As$ resembles the arrangement found in the Zn_3Y-type structure or its ternary variant, the $RhScSi_2$-type structure (*Pnma*) [34], with the

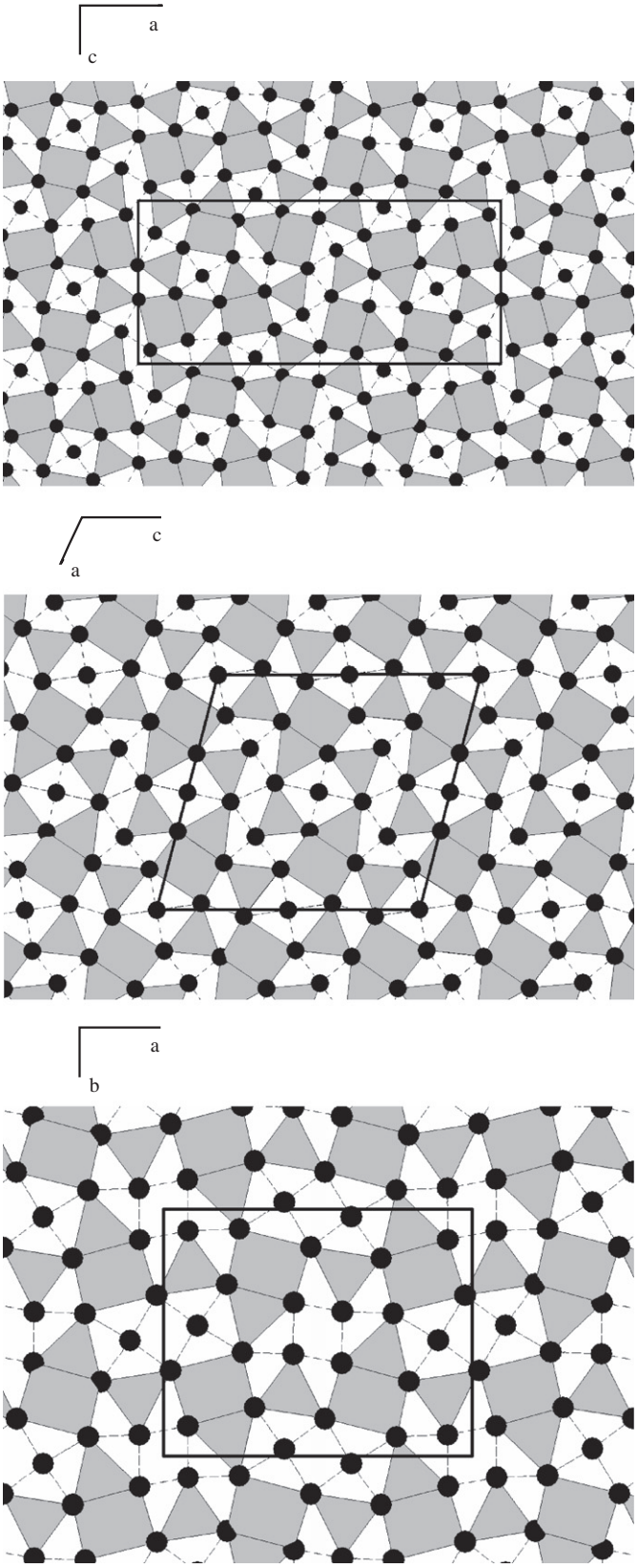

Fig. 2. The crystal structures of Hf_5As_3 and Nb_5As_3 (Nb_5As_3-type, *Pnma*) (top), Hf_7As_4 and Nb_7As_4 (Nb_7P_4-type, *C*2/*m*) (centre) and in Hf_2As (Ta_2P-type, *Pnnm*) (bottom) showing a combination of trigonal prisms (grey) and distorted bcc-fragments.

corresponding sites As–Si2, *M*1–Rh, *M*2–Si1 and *M*3–Sc. However, comparing the coordination polyhedra, considerable differences are found between the structure types. In the $RhScSi_2$-type

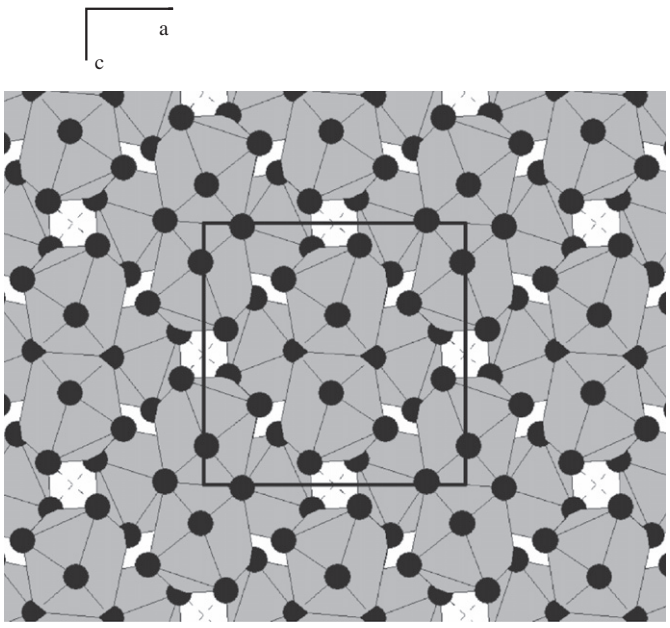

Fig. 3. The crystal structure of Nb_3As (Ti_3P-type, $P4_2/n$) showing a three-dimensional network of distorted square antiprisms centred by As.

structure Si1 and Si2 have almost similar coordination (tri-capped trigonal prisms), while the coordination of As and *M*2 in $Hf_{1.5+\delta}Nb_{1.5-\delta}As$ is completely different due to the relative shifts of the respective atomic positions. Thus, although space group, site symmetries and number of sites are identical for both structures, $Hf_{1.5+\delta}Nb_{1.5-\delta}As$ should be regarded as a structure type of its own due to considerable differences in chemistry and local coordination.

The refinement of site occupations showed considerable differences in the Hf/Nb ratio at the three different metal sites with 75% Nb occupation at the position *M*2, 49% Nb at *M*1 and only 7% Nb at *M*3 (Table 4). The refined composition of $Hf_{1.7}Nb_{1.3}As$ is in good agreement with the phase composition determined in the bulk sample (Table 6) which corresponds to the formula Hf3.25Nb2.75As2. The coordination polyhedra of the metal sites (based on the Wigner–Seitz cells) are shown in Fig. 4. Table 7 lists the refined site occupations together with site volumes (Wigner–Seitz cell volumes calculated with the program DIDO [35], and the PBOs calculated with covalence radii of Hf (144 pm), Nb (134 pm) and As (121 pm) [36] and considering the actual site occupation at the different metal positions. The site preferences observed in this compound can be understood qualitatively by considering size effects as well as metal–metal bonding interactions. Nb tends to occupy the sites with a smaller

Table 6
Phase compositions and lattice parameters of phases present in the section Hf_3As–Nb_3As.

Nominal sample composition (at% Hf/Nb/As)	Phase	Phase composition from EPMA (at% Hf/Nb/As)	Lattice parameters from powder XRD (Å)
80.3/0/19.7	Hf_3As, Ta_3As-type, $C2/c$	75.0/0.0/25.0	$a = 15.3965(2)$ $b = 5.37960(5)$ $c = 15.3376(2)$ $\beta = 90.2943(9)$
60.6/25.5/13.9	$Hf_{2+\delta}Nb_{1-\delta}As$, TiP_3-type, $P4_2/n$	66.3/8.7/25.0	$a = 10.7522(2)$ $c = 5.3703(2)$
40.2/39.9/19.9		53.0/21.9/25.1	$a = 10.6430(7)$ $c = 5.3848(6)$
40.2 / 39.9 / 19.9	$Hf_{1.5+\delta}Nb_{1.5-\delta}As$, own structure type, *Pnma*	40.6/34.5/24.9	$a = 7.1443(2)$ $b = 3.58542(9)$ $c = 11.6304(3)$
30.3/49.9/19.8		38.6/36.2/25.2	$a = 7.1351(2)$ $b = 3.5849(1)$ $c = 11.5991(4)$
21.9/49.0/29.1	(Nb_3As) TiP_3-type, $P4_2/n$	17.2/57.8/25.0	$a = 10.3255(3)$ $c = 5.2196(3)$
0/80.3/19.7		0/75.4/24.6	$a = 10.2943(2)$ $c = 5.19805(9)$

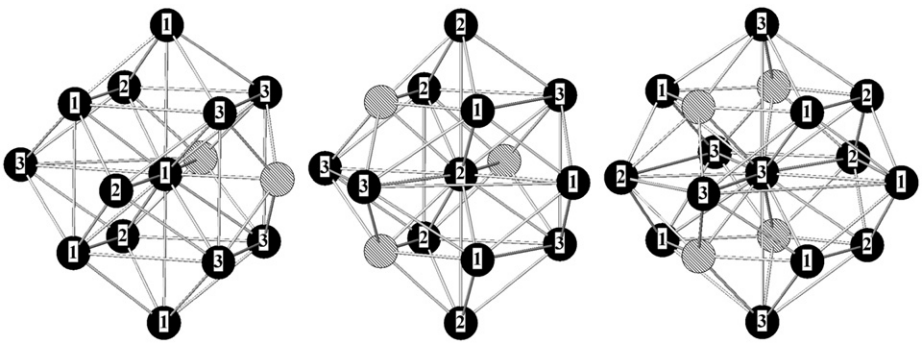

Fig. 4. Coordination polyhedra of the three different metal positions in $Hf_{1.5+\delta}Nb_{1.5-\delta}As$ as defined by the Wigner–Seitz cell. Left: *M*1 (0.49 Nb+0.51 Hf), centre: *M*2 (0.75 Nb+0.25 Hf), right *M*3 (0.07 Nb+0.93 Hf).

Table 7
Site occupations, site volumes and cumulated PBOs of metal positions in $Hf_{1.5+\delta}Nb_{1.5-\delta}As$ (own structure type, *Pnma*).

Site	Site occupation	Site volume (Å^3)	Sum of PBO[a] (all bonds)	Sum of PBO[a] (metal–metal bonds)
*M*1	0.49(1) Nb+0.51(1) Hf	20.08	4.39	3.53
*M*2	0.75(1) Nb+0.25(1) Hf	18.16	5.31	3.44
*M*3	0.07(1) Nb+0.93(1) Hf	19.90	4.51	1.90

[a] Calculated for the respective metal mixture at *M*1, *M*2, *M*3.

Table 8
Results from Rietveld refinement for the phase $Hf_{2+\delta}Nb_{1-\delta}As$.

Nominal sample composition: $Hf_{53.3}Nb_{26.7}As_{20}$					R_p: 4.15	R_{wp}: 5.62	
Background model: Chebyshev, 4th order					2θ-range (°): 10–120		
Main phase: $Hf_{2+\delta}Nb_{1-\delta}As$			Structure type: Ti_3P		Space group: $P4_2/n$ (86)		
Lattice parameters (Å)		$a = 10.6739(1)$	Cell volume (Å^3): 611.55(2)		Fraction: 84.2%	R_{Bragg}:1.88	
		$c = 5.36760(9)$					
Site	Mpl.	*x*	*y*	*z*	Atom	Site fr.	*B*(eq.)
*M*1	8	0.4150(1)	0.8943(1)	0.9612(3)	Hf	0.78(1)	0.3 (fixed)
					Nb	0.22(1)	
*M*2	8	0.3572(2)	0.5281(2)	0.7812(3)	Hf	0.90(1)	
					Nb	0.10(1)	
*M*3	8	0.3170(2)	0.7850(2)	0.4896(4)	Hf	0.59(1)	
					Nb	0.41(1)	
As	8	0.2988(3)	0.5387(3)	0.2894(6)	As	1	
Refined composition: $Hf_{2.27}Nb_{0.73}As$			Crystallite size (Lorenzian) [nm]: 53(1)		Preferred orientation spherical harmonics order: none		

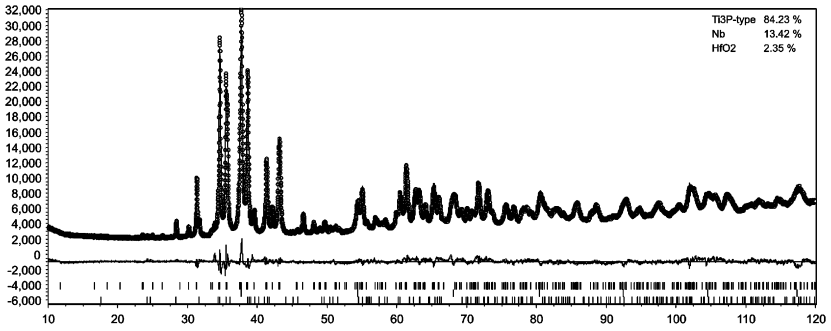

Fig. 5. Refined powder pattern of the sample with nominal composition $Hf_{53.3}Nb_{26.7}As_{20}$ containing 84.2% of $Hf_{2+\delta}Nb_{1-\delta}As$ (refined fraction). Experimental pattern: circles; modelled pattern: full line; difference between experimental and modelled pattern: full line, bottom.

site volume (as it is smaller than Hf) and sites with a larger amount of metal–metal bonding (Nb has an additional valence electron, and its larger enthalpy of sublimation [37] reflects its ability to form stronger metal–metal bonds). *M*2 is the smallest of the three sites and also shows a large sum of metal–metal PBOs (Table 7), so it is not surprising that it exhibits the largest site fraction of Nb. Although the *M*3 site has a slightly smaller volume than *M*1 (with 0.2 Å^3 difference), the sum of metal–metal PBOs is significantly larger for *M*1 explaining the relative preference of Nb for this position. A more quantitative treatment of site preferences in $Hf_{1.5+\delta}Nb_{1.5-\delta}As$, based on our DFT calculations, is given in Section 3.4.

3.2. Other phases in the section Hf_3As–Nb_3As

In addition to $Hf_{1.5+\delta}Nb_{1.5-\delta}As$, the ternary compound $Hf_{2+\delta}Nb_{1-\delta}As$ with Ti_3P-type structure was found to exist in the section Hf_3As–Nb_3As. This compound is isostructural to binary Nb_3As and exists in the composition range of $(0.12<\delta<0.65)$ according to our EPMA results. Nb_3As itself also exhibits extended solubility for Hf with a limiting composition of approx. 17 at% Hf corresponding to the formula $Hf_{0.68}Nb_{2.32}As$. In contrary solubility of Nb in Hf_3As (Ta_3As-type structure) appears to be limited (definitely less than 5 at%) and this compound was not detected in any ternary sample investigated. Phase compositions and lattice parameters of the M_3As-phases with the respective limiting compositions are given in Table 6. It is estimated that the phase compositions determined by EPMA are accurate within ± 1 at.%.

The fact that two separate phase fields with Ti_3P-type structure exist in the section Hf_3As–Nb_3As raises several questions. Firstly, it cannot be ruled out that a complete solid solution between the two phase fields exists at a temperature different from 1400 °C. This would mean that the intermediate phase $Hf_{1.5+\delta}Nb_{1.5-\delta}As$ does only exist in a certain temperature range, e.g. as high temperature phase. On the other hand, the existence of a ternary phase field separated from the solid solution based on binary Nb_3As could also be connected to a stabilization of the specific composition around $Hf_{2+\delta}Nb_{1-\delta}As$ due to partial ordering. In any case, information on site occupation in ternary $Hf_{2+\delta}Nb_{1-\delta}As$ would be quite helpful to analyse the situation.

No single crystal suitable for structure investigation could be found in the samples containing $Hf_{2+x}Nb_{1-x}As$, so it was decided to use Rietveld refinement of powder XRD data for the determination of site occupations. The results from Rietveld refinement for a sample with the nominal composition

Table 9
Site occupations, site volumes and cumulated PBOs of metal positions in $Hf_{2+\delta}Nb_{1-\delta}As$ (Ti_3P-type, $P4_2/n$).

Site	Site occupation	Site volume (Å^3)	Sum of PBO[a] (all bonds)	Sum of PBO[a] (metal–metal bonds)
*M*1	0.22(1) Nb+0.78(1) Hf	21.00	4.16	2.99
*M*2	0.10(1) Nb+0.90(1) Hf	19.30	5.37	2.55
*M*3	0.41(1) Nb+0.59(1) Hf	19.68	4.66	3.07

[a] Calculated for the respective metal mixture at *M*1, *M*2, *M*3.

Table 10
End member energies for the Ta_3As-type structure obtained by DFT calculations (only pure Hf_3As and monosubstituted end members were considered).

End member (sublattice notation)	*x*	Formation energy per mol of atoms (kJ)
(Hf:Hf:Hf:Hf:Hf:Hf:As)	**0**	**−61.31**
(Nb:Hf:Hf:Hf:Hf:Hf:As)	0.5	−56.25
(Hf:Nb:Hf:Hf:Hf:Hf:As)	0.5	−56.67
(Hf:Hf:Nb:Hf:Hf:Hf:As)	0.5	−56.43
(Hf:Hf:Hf:Nb:Hf:Hf:As)	0.5	−55.96
(Hf:Hf:Hf:Hf:Nb:Hf:As)	0.5	−58.17
(Hf:Hf:Hf:Hf:Hf:Nb:As)	**0.5**	**−58.61**

Table 11
End member energies for the Ti_3P-type structure obtained by DFT calculations.

End member (sublattice notation)	*x*	Formation energy per mol of atoms (kJ)
(Hf:Hf:Hf:As)	**0**	**−61.02**
(Nb:Hf:Hf:As)	1	−51.57
(Hf:Nb:Hf:As)	1	−50.75
(Hf:Hf:Nb:As)	**1**	**−56.88**
(Hf:Nb:Nb:As)	2	−42.72
(Nb:Hf:Nb:As)	**2**	**−48.41**
(Nb:Nb:Hf:As)	2	−45.21
(Nb:Nb:Nb:As)	**3**	**−40.87**

Table 12
End member energies for the $Hf_{1.5+\delta}Nb_{1.5-\delta}As$-type structure obtained by DFT calculations.

End member	*x*	Formation energy per mol of atoms (kJ)
(Hf:Hf:Hf:As)	**0**	**−60.14**
(Nb:Hf:Hf:As)	1	−54.71
(Hf:Nb:Hf:As)	**1**	**−57.04**
(Hf:Hf:Nb:As)	1	47.47
(Hf:Nb:Nb:As)	2	−44.85
(Nb:Hf:Nb:As)	2	−38.44
(Nb:Nb:Hf:As)	**2**	**−56.68**
(Nb:Nb:Nb:As)	**3**	**−41.97**

$Hf_{53.3}Nb_{26.7}As_{20}$ are shown in Table 8. A graphical representation of the experimental powder pattern and the comparison with the results of refinement is given in Fig. 5. The sample contained 84.2% of $Hf_{2+\delta}Nb_{1-\delta}As$ (refined fraction), 13.4% (Nb) and 2.4% HfO_2. The results listed in Table 8 show different occupation at the three metal sites with Nb present at all metal sites, but preferably entering the *M*3 site. The consideration of site volumes and PBOs listed in Table 9 does not allow a straightforward interpretation of site preferences in this compound. The relative preference of Nb for position *M*3 meets expectations, as this position shows the largest sum of M–M PBOs and it is only 0.4 Å larger than the tightest position *M*2. On the other hand, the preferred occupation of the tightest position *M*2 with Hf could be only supported by the lowest sum of M–M PBOs for this site. Again it may be concluded that the combination of thermodynamic modelling with DFT calculations discussed in Sections 3.3 and 3.4. allows a much better theoretical description of experimental site fractions.

3.3. Modelling of ground state energies

The ground state energies for the end members of the Hf_3As-, Nb_3As- and $Hf_{1.5+\delta}Nb_{1.5-\delta}As$- structures were calculated using the procedures described in Section 2.2. with the sublattices defined according to the crystal structure data listed in Tables 1–4. Each geometrically independent metal site was defined as a sublattice of its own and all arsenic sites were included in one sublattice. The respective sublattice notations are thus (*M*1:*M*2:*M*3:As) for Nb_3As and $Hf_{1.5+\delta}Nb_{1.5-\delta}As$ and (*M*1:*M*2:*M*3:*M*4:*M*5:*M*6:As) for Hf_3As. The number of end members to be considered is 8 (2^3) for (*M*1:*M*2:*M*3:As) and 64 (2^6) for (*M*1:*M*2:*M*3:*M*4:*M*5:*M*6:As). In order to reduce the calculation time, only the pure and the monosubstituted end members were calculated for Hf_3As. The binary structures were allowed to relax their cell parameters and atom positions, but in order to save the computation time, the atom positions taken from the relaxation of the binaries were kept in the monosubstituted ones (the cell parameters were still set free). The calculated end members energies were first recalculated to the energy per formula unit (by dividing by the number of formula unit in the unit cell) and then to the formation energy per formula unit by subtracting the energy of a stoichiometric mixture of the pure element's energies per atom. The results of DFT energy calculations are given in Tables 10–12. The most stable end member for each ternary composition is highlighted in bold letters. The composition parameter *x* is defined according to the general formula $Hf_{3-x}Nb_xAs$ defining the whole section Hf_3As–Nb_3As.

The comparison of end member energies for the different phases allows a qualitative prediction of site preferences as well as the analysis of phase stabilities at 0 K. In case of Nb_3As and $Hf_{1.5+\delta}Nb_{1.5-\delta}As$ all eight end members have been calculated and their energies can be directly compared. The most stable end member energies as highlighted in Tables 11 and 12 point to a preference of Nb for *M*3 and Hf for *M*2 in case of Nb_3As and $Hf_{2+\delta}Nb_{1-\delta}As$ which is in agreement with experimental findings. In case of $Hf_{1.5+\delta}Nb_{1.5-\delta}As$, a preference of Nb for *M*2 and Hf for *M*3 is predicted, this again agrees well with the refined site occupations. For Hf_3As no experimental site occupation data are available as this phase was not found in any of the ternary samples. The energies listed in Table 10 show that Nb should preferably enter positions *M*6 and *M*5 in a possible limited solubility range.

For the analysis of phase stabilities at 0 K, the most stable end members for each phase and each composition were plotted in Fig. 6. While the energies for Nb_3As and $Hf_{1.5+\delta}Nb_{1.5-\delta}As$ were taken directly from Tables 11 and 12, the energies for Hf_3As were calculated from the monosubstituted end members (Table 10)

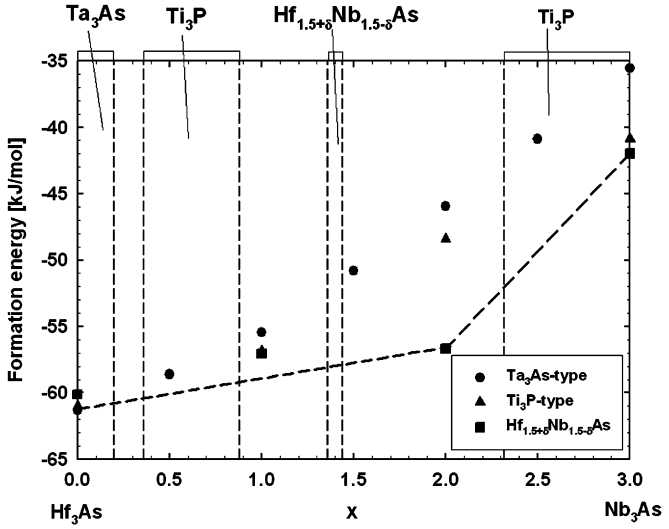

Fig. 6. A comparison of the most stable end member energies for the three phases based on the structures of Hf_3As (Ta_3As-type), Nb_3As (Ti_3P-type) and $Hf_{1.5+\delta}Nb_{1.5-\delta}As$ as a function of composition. The composition parameter x corresponds to the general formula $Hf_{3-x}Nb_xAs$.

Table 13
Energies for the most stable end members of Ta_3As-structure type in the Hf_3As–Nb_3As section, calculated with the assumption of the independent substitution.

End member (sublattice notation)	x	Formation energy per mol of atoms (kJ)
(Hf:Hf:Hf:Hf:Hf:Hf:As)	**0**	−61.31
(Hf:Hf:Hf:Hf:Hf:**Nb**:As)	0.5	−58.61
(Hf:Hf:Hf:Hf:**Nb**:Nb:As)	1	−55.47
(Hf:**Nb**:Hf:Hf:Nb:Nb:As)	1.5	−50.83
(Hf:Nb:**Nb**:Hf:Nb:Nb:As)	2	−45.95
(**Nb**:Nb:Nb:Hf:Nb:Nb:As)	2.5	−40.89
(Nb:Nb:Nb:**Nb**:Nb:Nb:As)	3	−35.54

with the approximation of independent substitution and the resulting most stable end members are given in Table 13. It was already demonstrated for Ge-systems [17,18] that the assumption of independent substitution yields reasonable results.

In agreement with our experimental results at 1400 °C, the Ta_3As type was found to be the most stable structure for binary Hf_3As, while for binary Nb_3As the $Hf_{1.5+\delta}Nb_{1.5-\delta}As$-type structure was found to be more stable (by 1.1 kJ/mol) than the Ti_3P-type found experimentally at 1400 °C. This could be a hint that Nb_3As exists in two modifications with the known Ti_3P-type phase being only stable at high temperatures. Connecting the most stable end members with a line as shown in Fig. 6, in can bee seen that one additional ternary ordered compound Nb_2HfAs with the configuration (Nb:Nb:Hf:As) and $Hf_{1.5+\delta}Nb_{1.5-\delta}As$-type structure is predicted to exist at 0 K. The experimentally observed phase fields at 1400 °C, especially the existence of a Hf-rich phase field with Ti_3P-type structure is not directly supported by the calculated ground state energies.

3.4. Thermodynamic modelling

For the thermodynamic modelling of site fractions, only the Ti_3P- and $Hf_{1.5+\delta}Nb_{1.5-\delta}As$-type structures were considered, as no experimental site occupation data exist for Ta_3As-type Hf_3As and so no comparison with the model is possible in this case. The frame of reference was constructed as a sum of site-fraction

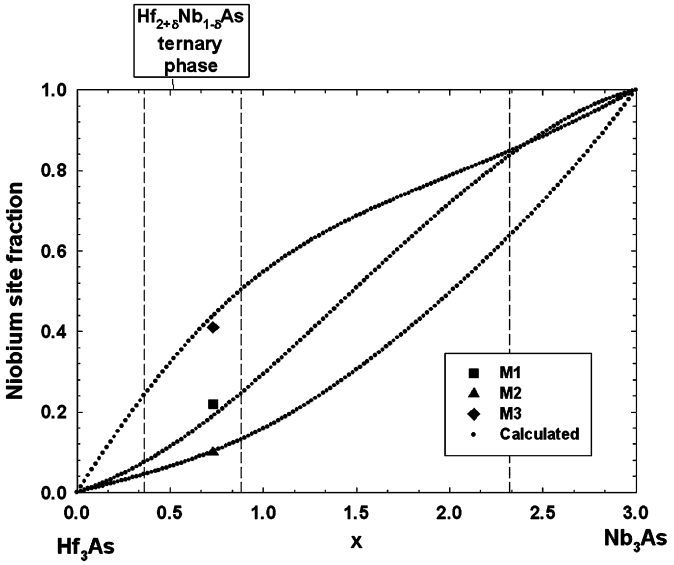

Fig. 7. Comparison of modelled Nb-site fractions (small symbols) for the Ti_3P-type structure with experimental data determined by Rietveld refinement of powder data for $Hf_{2+\delta}Nb_{1-\delta}As$ (large symbols). The composition parameter x corresponds to the general formula $Hf_{3-x}Nb_xAs$.

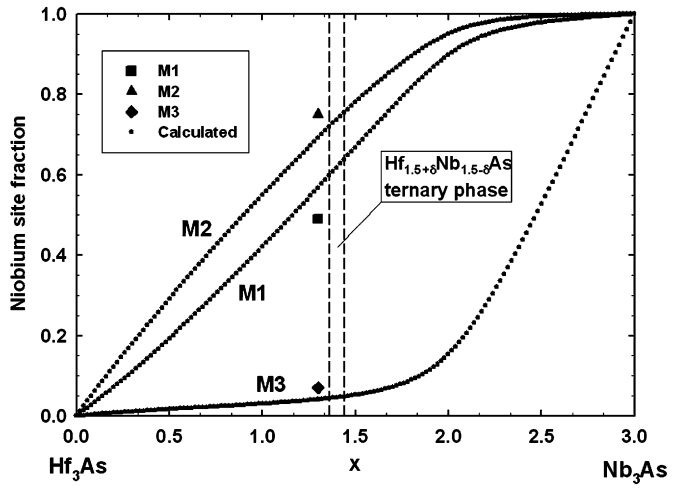

Fig. 8. Comparison of modelled Nb-site fractions (small symbols) for the $Hf_{1.5+\delta}Nb_{1.5-\delta}As$-type structure with experimental data determined by single crystal XRD for $Hf_{1.5+\delta}Nb_{1.5-\delta}As$ (large symbols). The composition parameter x corresponds to the general formula $Hf_{3-x}Nb_xAs$.

weighed end member ground state energies according to Eq. (2). For example, the end member (Hf:Nb:Hf:As) contributes with the factor $y_{Hf}^{M1}y_{Nb}^{M2}y_{Hf}^{M2}\cdot G(Hf:Nb:Hf:As)$ to the frame of reference. Considering the ideal entropy of mixing at 1673 K (Eq. (3)) and neglecting any excess contribution to the Gibbs energy, the equilibrium site fractions were modelled by Gibbs energy minimization as a function of composition. The resulting site fractions for both structure types are shown together with experimental data in Figs. 7 and 8. It can be seen that the model predictions are in excellent agreement with experiments in both cases.

For the Ti_3P-type structure, two separate phase fields exist, but experimental site fractions are only available for the Hf-rich ternary phase field. According to the thermodynamic model shown in Fig. 7, a change of site preferences is predicted for the composition range of the solid solution Nb_3As; i.e. the clear separation of *M*1 and *M*3 site occupancies is predicted to vanish

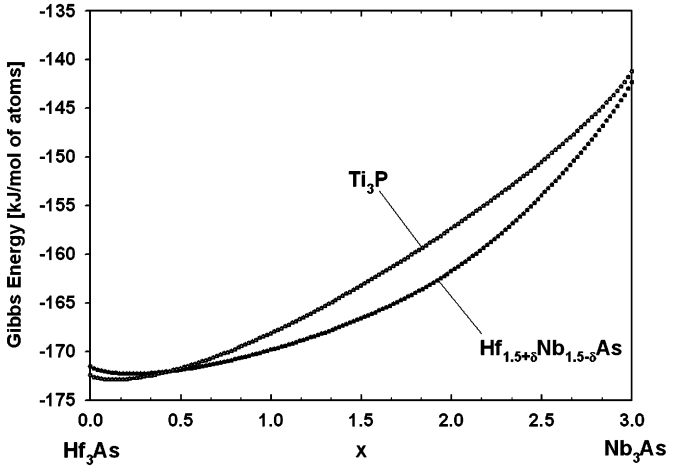

Fig. 9. Gibbs energy per mole of atoms for Ti_3P-type and $Hf_{1.5+\delta}Nb_{1.5-\delta}As$-type solid solutions determined by thermodynamic CEF modelling. The composition parameter x corresponds to the general formula $Hf_{3-x}Nb_xAs$.

and similar occupation factors of these two sites should be observed in the Nb-rich solid solutions. It would be interesting to test this prediction with a structure refinement in this solid solution, but up to now we were not successful to isolate a suitable single crystal.

In the relatively small phase field of $Hf_{1.5+\delta}Nb_{1.5-\delta}As$, the clear preference of Hf for position *M*3 is well predicted by the thermodynamic model (Fig. 8). The modelled Nb-site fraction is slightly underestimated for *M*2 and slightly overestimated for *M*1, but the general trend is very well reproduced by the model. Note that the phase boundaries given in Figs. 7 and 8 correspond to our EPMA analyses of bulk samples while the compositions of the experimental site fraction data are refined from diffraction data. The small difference of the refined composition of $Hf_{1.5+\delta}Nb_{1.5-\delta}As$ (single crystal) and the respective phase boundary probably reflects the combined experimental error of the two separate experiments, or it may be due to a different composition of the selected single crystal (isolated from the sample surface) and the average bulk material.

The modelled Gibbs energies for both structure types within the entire section Hf_3As-Nb_3As are shown in Fig. 9. According to our model, the $Hf_{1.5+\delta}Nb_{1.5-\delta}As$-type solid solution is predicted to be stable in the entire composition range between binary Nb_3As and $Hf_{2.4}Nb_{0.6}As$, while the stability range of the Ti_3P-type solid solution is restricted to a small area at the Hf-rich side. Note that in agreement with experimental results, the Ta_3As-type (which is not included in Fig. 9) is predicted to be the most stable phase for binary Hf_3As according to our DFT calculations.

Considering these results it may be concluded that the modelled Gibbs energies in the present form are not accurate enough to predict the correct phase relations in the entire section. While the phase relations at the Hf-rich end are well predicted by the model (Ta_3As-type followed by Ti_3P-type solid solution), the range of existence for the $Hf_{1.5+\delta}Nb_{1.5-\delta}As$-type solid solution is by far overestimated. Thus, the excess Gibbs energy term of the CEF model as given in Eq. (1) would be essential to yield correct results in a CALPHAD-type modelling of phase relations.

It is interesting to compare this result with our previous modelling in the section Zr_5Ge_4–Hf_5Ge_4 which consists of two solid solutions based on binary Hf_5Ge_4 (structure type: Sm_5Ge_4, *Pnma*) and Zr_5Ge_4 (structure type: Zr_5Si_4, $P4_12_12$) [18]. In this case, site occupations as well as the position of the two-phase field could be predicted very well with a similar model approach. The basic difference to the section discussed here, however, is the very close structural relationship between the two structure types of Hf_5Ge_4 and Zr_5Ge_4 which apparently allows neglecting any excess Gibbs energy term (e.g. vibrational or electronic contributions to the entropy) if the energies of the two structures are directly compared. Therefore, it is possible to use 0 K ground state energies in combination with an ideal entropy term to predict the relative energies of the two solid solutions even at elevated temperatures. In the case of the Ti_3P- and the $Hf_{1.5+\delta}Nb_{1.5-\delta}As$-type structures, we are comparing two structures with quite different structural features, so an excess Gibbs energy term is obviously necessary for an accurate comparison of energies at elevated temperatures. Nevertheless, it should be pointed out that the simplified approach of using ground state energies in combination with the ideal entropy of mixing is still a very valuable tool for the prediction of site occupations as a function of composition and for the basic determination of the substitution energies.

Acknowledgments

Financial support from the Austrian Science Foundation (FWF) under the Project number P16946-N11 is gratefully acknowledged. The authors wish to thank Herta Effenberg for her help with the single crystal X-ray diffraction and Herbert Ipser for many fruitful discussions.

References

[1] W. Jeitschko, H. Nowotny, Monatsh. Chem. 93 (1962) 1284–1287.
[2] H. Boller, E. Parthé, Acta Cryst. 16 (1963) 1095–1101.
[3] S. Rundqvist, B. Carlsson, Acta Chem. Scand. 22 (1968) 2395–2396.
[4] J.O. Willerström, B. Carlsson, S. Rundqvist, J. Solid State Chem. 31 (1980) 227–232.
[5] B. Carlsson, S. Rundqvist, Acta Chem. Scand. 25 (1971) 1742–1752.
[6] S. Laohavanich, S. Thanomkul, S. Pramatus, Acta Cryst. B 37 (1981) 227–228.
[7] S. Rundqvist, B. Carlsson, C. Pontchour, Acta Chem. Scand. 23 (1969) 2188–2190.
[8] R.M. Waterstrat, K. Yvon, H.D. Flack, E. Parthe, Acta Cryst. B 31 (1975) 2765–2769.
[9] H.F. Franzen, M. Köckerling, Prog. Solid State Chem. 23 (1995) 265–289.
[10] H. Kleinke, Trends Inorganic Chem. 7 (2001) 135–149.
[11] C.-S. Lee, E. Dashjav, H. Kleinke, J. Alloys Comp. 338 (2002) 60–68.
[12] A. Assoud, S. Derakhshan, K.M. Kleinke, H. Kleinke, J. Solid State Chem. 179 (2006) 464–469.
[13] K.W. Richter, Monatsh. Chem. 136 (2005) 1885–1897.
[14] K.W. Richter, H. Flandorfer, H.F. Franzen, J. Solid State Chem. 167 (2002) 517–524.
[15] K.W. Richter, H.F. Franzen, J. Solid State Chem. 150 (2000) 347–355.
[16] K.W. Richter, R. Picha, H. Ipser, H.F. Franzen, Solid State Sci. 5 (2003) 653–662.
[17] P. Warczok, F. Mittendorfer, G. Kresse, A. Kroupa, H. Ipser, K.W. Richter, Solid State Sci. 9 (2007) 159–165.
[18] N. Ponweiser, P. Warczok, C.L. Lengauer, K.W. Richter, Solid State Sci 11 (2009) 395–401.
[19] TOPAS, Bruker AXS Inc., Karlsruhe, Germany, 1999.
[20] Z. Otwinowski, D. Borek, W. Majewski, W. Minor, Acta Cryst. A 59 (2003) 228–234.
[21] G.M. Sheldrick, SHELX-97, University of Göttingen, 1997.
[22] B. Sundman, J. Agren, J. Phys. Chem. Solids 42 (1981) 297–301.
[23] V.P. Thermo-Calc, Software for Thermodynamic Calculations in Multicomponent Systems, Thermo-Calc AB, Stockholm, Sweden, 2003.
[24] A. Dinsdale, CALPHAD 15 (1991) 317–425.
[25] G. Kresse, J. Furthmüller, Comput. Mater. Sci. 6 (1996) 15–50.
[26] G. Kresse, J. Hafner, Phys. Rev. B 47 (1993) 558–561.
[27] W.H. Press, B.P. Flannery, S.A. Teukolsky, W.T. Vetterling, Numerical Recipies, Cambridge University Press, New York, 1986.
[28] P.E. Blöchl, Phys. Rev. B 50 (1994) 17953–17979.
[29] G. Kresse, D. Joubert, Phys. Rev. B 59 (1999) 1758–1775.
[30] J.P. Perdew, J.A. Chevary, S.H. Vosko, K.A. Jackson, M.R. Pederson, D.J. Singh, C. Fiolhais, Phys. Rev. B 46 (1992) 6671–6687.
[31] H.J. Monkhorst, J.D. Pack, Phys. Rev. B 13 (1976) 5188–5192.
[32] P.E. Blöchl, O. Jepsen, O.K. Andersen, Phys. Rev. B 49 (1994) 16223–16233.
[33] P. Warczok, H. Ipser, K.W. Richter, publication in preparation, 2009.
[34] B. Chabot, H.F. Braun, K. Yvon, E. Parthé, Acta Cryst. B 37 (1981) 668–671.
[35] E. Koch, W. Fischer, Z. Kristallogr. 211 (1996) 251–253.
[36] J. Emsley, The Elements, Clarendon Press, Oxford, 1989.
[37] R. Hultgren, P.D. Desai, D.T. Hawkins, M. Gleiser, K.K. Kelley, D.D. Wagman, Selected Values of the Thermodynamic Properties of the Elements, ASM, Ohio, 1973.